PERGAMON

International Journal of Heat and Mass Transfer 44 (2001) 1699–1709

International Journal of HEAT and MASS TRANSFER

www.elsevier.com/locate/ijhmt

On the transition from conduction to convection regime in a cubical enclosure with a partially heated wall

Ramón L. Frederick *, Fernando Quiroz

Departamento de Ingeniería Mecánica, Universidad de Chile, Casilla 2777, Santiago, Chile

Received 13 January 2000; received in revised form 22 June 2000

Abstract

Steady-state laminar natural convection in a cubical enclosure with a cold vertical wall and a hot square sector on the opposite wall is numerically studied. The flow pattern consists of a single, symmetric circulation cell. The transition from conduction to convection regime ends at $Ra = 10^5$, and is characterized by conduction suppression and slow development of convection. In the range of $Ra = 10^5$–10^7, lateral velocities become very large, producing a highly mixed, thermally stratified three-dimensional flow, and the circulation cell undergoes cross-sectional changes. In the whole range of *Ra*, the Nusselt number is reduced compared to the case in which the full side wall is hot (test case).

1. Introduction

Natural convection in enclosures continues to be a very active area of research. There is abundant numerical work in this area using two-dimensional solutions. However, any assumption of two-dimensionality is only an approximation to the actual behavior, which is always three-dimensional. Not all the problems of confined natural convection possess a two-dimensional version, and when it can be defined, the degree of compliance of the flow to the two-dimensional assumption varies in the range of Rayleigh number. A three-dimensional approach, being more realistic, can detect phenomena not seen in the two-dimensional version. Since the works of Fusegi et al. [1], Janssen et al. [2], Lee and Lin [3] and others, three-dimensional numerical solutions often appear in the literature. These authors have studied flow structures, thermal fields, and stability conditions in vertical and inclined cubical enclosures with sidewall heating and cooling.

At variance with the sidewall heated case (test problem) [1,2], miniaturization of electronic components often leads to the designing of systems with active surfaces of different areas. The inequality in the size of the sources causes delays in the transition from conduction to convection regime to higher Rayleigh numbers relative to the test problem. As buoyancy forces on the fluid depend on the size of the active sources, fluid mixing in the core of the enclosure is made difficult. Well-mixed fluid, characteristic of a fully convective regime, is attained at higher values of *Ra* than in the test case. A Rayleigh number of 4×10^5 has been proposed for the onset of the fully convective regime in some situations [4,5]. In the test case, convective regime apparently sets in at a Rayleigh number of 10^3.

Three-dimensional studies originating from applications to the cooling of electronic components, often use conditions of prescribed heat flux [6–8]. This condition, although realistic in that field, does not allow a comparison of flow and heat transfer mechanisms and their dependence on *Ra* with the ones found in the test problem. Little attention has been given to three-dimensional cases, lacking a two-dimensional counterpart, with isothermal active surfaces. These cases are of fundamental and practical importance, because the relative position of the active sources, as well as their size,

* Corresponding author. Tel.: +56-2-678-4448; fax: +56-2-698-8453.

E-mail address: rfrederi@cec.uchile.cl (R.L. Frederick).

0017-9310/01/$ - see front matter
PII: S0017-9310(00)00219-2

Nomenclature

C	constant in Nu–Ra relationships
g	gravity constant
L	cavity side
n	exponent in Nu–Ra relationships
Nu	overall Nusselt number
Pr	Prandtl number (v/α)
Ra	Rayleigh number ($g\beta\Delta TL^3/v\alpha$)
s	side of the square hot sector
T_H, T_C	hot and cold wall temperatures
U, V, W	dimensionless velocities in the X, Y and Z directions, respectively
X, Y, Z	dimensionless coordinates

Greek symbols

α	thermal diffusivity
β	thermal expansion coefficient
ΔT	overall temperature difference, $(T_H - T_C)$
Θ	dimensionless temperature
v	kinematic viscosity
ρ	density

Subscripts

i, j	indexes for velocities and coordinates. $U_1 = U$, $U_2 = V$, $X_1 = X$, $X_2 = Y$, etc.
av	average
max	maximum value (in velocities)

determine the circulation modes, temperature fields and heat transfer. Poulikakos [9] studied the two-dimensional natural convection in a rectangular cavity with hot and cold elements of equal size on the same vertical wall. Kuhn and Oosthuizen [10] studied the two-dimensional transient natural convection in a partially heated rectangular cavity, in which the position of the heating element was varied. The same situation had been experimentally investigated earlier by Turner and Flack [11]. Gatheri et al. [12], simulated the three-dimensional turbulent natural convection in a room with a heater and a window on the same wall. Frederick [5] studied the laminar natural convection in a cubical enclosure with hot and cold sources located side by side on a vertical wall. For the problems discussed in [5,12], a two-dimensional counterpart does not exist.

In this paper, we study the steady-state, laminar natural convection in a cubical enclosure with two active surfaces of unequal areas and imposed temperatures, located on vertical, opposite walls. The hot source is smaller than the cold one, which covers a vertical wall completely. This fully three-dimensional problem will be treated in the simplest possible geometry, with a flush mounted square heater centered on the corresponding vertical wall, in order to minimize the number of geometric parameters. The objectives of this paper are of fundamental and applied nature. First, to provide the heat transfer results for this case as a function of the Rayleigh number in the laminar regime. Then the criteria to characterize the transition from conduction to convection regime will be examined. The transition will be described in terms of the usual criteria and also by the variations in an average fluid temperature in the enclosure, in the range of the Rayleigh number covered. An explanation of the heat transfer behavior will be given in terms of the temperature fields and flow patterns, which vary with Ra. Finally, a delimitation of the features that can be explained on two- and three-dimensional grounds will be given.

2. Formulation

The physical situation is depicted in Fig. 1. A cubical cavity of the side L contains air ($Pr = 0.71$). The hot source is a non-protruding square sector of side s at temperature T_H, centered on the wall at $X = 0$. The wall at $X = 1$ acts as a cold surface at temperature T_C. All other sectors of the cavity walls are adiabatic. The ratio s/L will be given values of 0.3, 0.5 and 0.7. The case $s/L = 1.0$ is the side wall heated cavity problem, and will be referred to as the test problem, whose solution has been extensively reported [1,2].

Steady-state results will be given. Earlier evidence [2], shows that in the test problem, time-dependent flows may occur at the Rayleigh numbers slightly above 10^6 with air as the test fluid. The dimensionless governing equations of continuity (1), momentum (2) and energy (3) in their steady-state form for laminar flow of an incompressible Boussinesq fluid inside the cavity are, respectively:

$$\frac{\partial U_j}{\partial X_j} = 0, \tag{1}$$

$$U_j \frac{\partial U_i}{\partial X_j} = -\frac{\partial P}{\partial X_i} + Pr \frac{\partial^2 U_i}{\partial X_j \partial X_j} + Ra_i Pr \Theta, \tag{2}$$

$$U_j \frac{\partial \Theta}{\partial X_j} = \frac{\partial^2 \Theta}{\partial X_j \partial X_j}, \tag{3}$$

where $Ra_2 = Ra$ is the Rayleigh number and $Ra_1 = Ra_3 = 0$. The cube side is retained in the definition of the Nusselt and Rayleigh numbers for all values of s/L in order to allow an easy comparison with the test case. The equations are made dimensionless using L, α, ρ and ΔT as reference quantities. All velocities are zero at the walls. The dimensionless temperature Θ is defined to have values of 0.5 and −0.5 at the hot and cold sources, respectively. The temperature boundary conditions are:

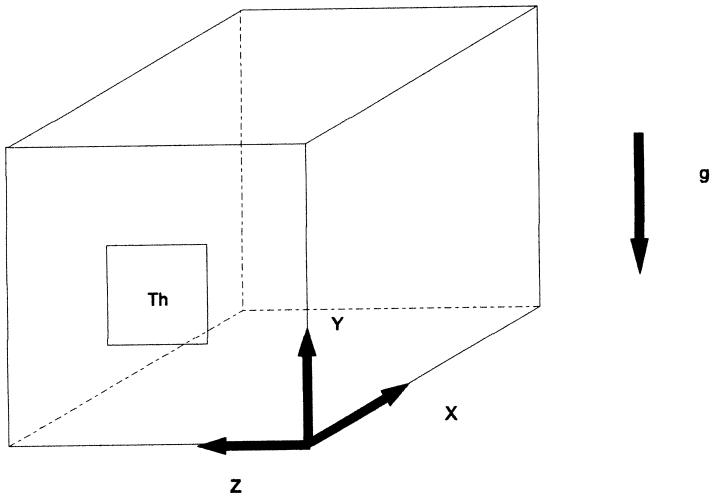

Fig. 1. Physical situation and coordinates.

1. $\Theta = 0.5$ at $X = 0, (1 - s/L)/2 \leqslant Y \leqslant (1 + s/L)/2$, $(1 - s/L)/2 \leqslant Z \leqslant (1 + s/L)/2$.
2. $\Theta = -0.5$ at $X = 1$.
3. $\partial\Theta/\partial X_i = 0$ elsewhere on the walls.

3. Numerical method

The standard SIMPLER method with a power law discretization was used. Staggered grids were deployed with vertical velocity nodes (V) at the walls $Y = 0$ and $Y = 1$ (bottom and top). The planes $X = 0$, $X = 1$ (left and right) and $Z = 0$, $Z = 1$ (front and back) contain U and W nodes, respectively. No temperature and pressure nodes are provided on the physical borders of the enclosure, but external (virtual) nodes for these variables are added in six planes parallel to the physical borders at a half control volume distance from them.

On the active sectors, temperatures were first imposed on the external nodes. For solving the energy equation, the half control volume outside the physical border was assigned an infinite diffusion coefficient. The discretization coefficient linking the temperature of the first internal node to the temperature of the neighboring virtual node was calculated using Patankar's harmonic mean rule [13]. In this way, the externally imposed temperature was rapidly transferred to the physical border during the iterative solution of the energy equation. Similar procedures were used to evaluate the discretization coefficients in the momentum equations, for U at the horizontal and back/front walls, for V at the right/left and back/front walls, and for W at the horizontal and right/left walls. Adiabaticity conditions were imposed by equating the temperatures of consecutive grid points at both sides of the physical border.

Uniform, staggered grids of $62 \times 62 \times 62$ nodes were used throughout. These grids provided accurate, steady solutions to the test problem for Rayleigh numbers of 10^3–10^7. Excellent agreement was found with the results by Fusegi et al. [1]: at $Ra = 10^6$, the maximum velocities U and V in the plane of symmetry $Z = 0.5$ differed from the ones in [1] by +0.46 and −2.23%, respectively, while the overall Nusselt number differed by 0.74%. No signs of numerical instability were found in the whole ranges of Ra and s/L. The solutions converged to apparently steady values in all variables. Convergence was assumed to be obtained when the overall Nusselt numbers from two consecutive general iterations did not differ by more than 1.5×10^{-5}. The overall Nusselt number was computed on the vertical mid-plane $X = 0.5$, to avoid possible heat flux singularities at the perimeter of the hot sector.

4. Results and discussion

The flow and temperature fields are completely symmetric with respect to the plane $Z = 0.5$. A description of these fields will be better understood if we first examine the overall parameters and then, we describe the flow mechanisms. Fig. 2 shows curves of the Nusselt vs Rayleigh number for $s/L = 0.3$, 0.5 and 0.7, together with the curve for the test problem, (Fusegi et al. [1], $s/L = 1.0$). For the $s/L < 1$, the overall Nusselt numbers are lower than those for the test problem. Nu always grows with s/L at a given Ra. Fusegi's results form a single straight line in a log-log plot over the Rayleigh number range (10^3–10^7), suggesting a predominantly convective behavior. The Nusselt numbers for other values of s/L (specially $s/L = 0.3$ and 0.5) increase slowly

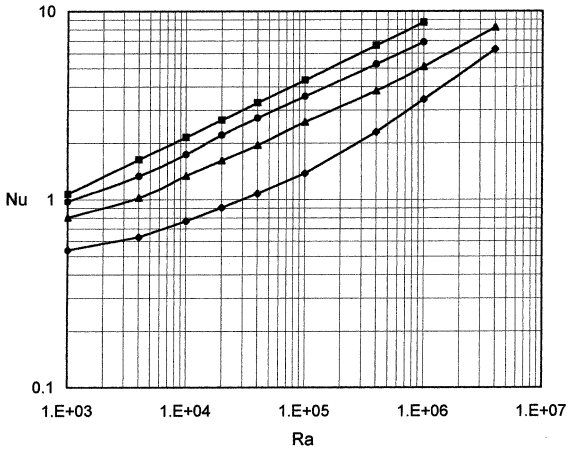

Fig. 2. Overall Nusselt number as a function of *Ra*. Curves from top to bottom: $s/L = 1.0$ (test problem), $s/L = 0.7$, 0.5 and 0.3.

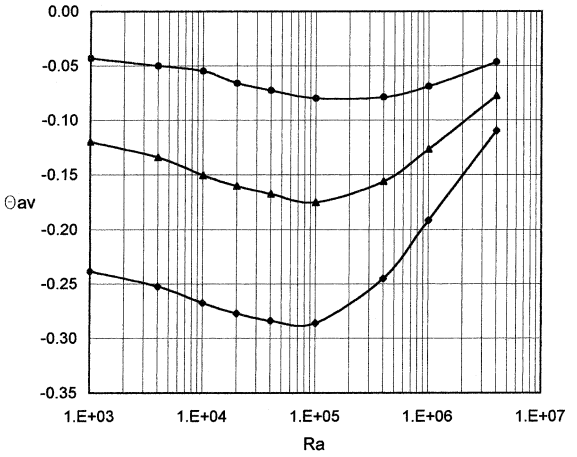

Fig. 3. Average fluid temperature as a function of *Ra*. Curves from top to bottom: $s/L = 0.7$, 0.5 and 0.3.

at low *Ra*, suggesting a delay in the transition to the convective regime. From the overall heat transfer curves, a definite point of transition from conduction to convection regime is difficult to assign.

In problems with active surfaces of imposed temperatures and different areas, an arithmetic average (Θ_{av}) of the dimensionless temperatures in the enclosure nodes, excluding the walls, can be defined. This average is not directly related to the concept of the "cup mixing temperature" used in channel flow. Even though in the test problem Θ_{av} would be constant and equal to the arithmetic average of the active wall temperatures at all Rayleigh numbers, when active areas are unequal, Θ_{av} varies with *Ra* and takes values nearer to the temperature of the bigger active surface. We postulate that the sensitivity of Θ_{av} to changes in *Ra* makes it a useful and concise index of the state of the temperature field. Fig. 3 shows the variation of Θ_{av} with *Ra* for the three values of s/L. For a given *Ra*, Θ_{av} grows with s/L, as expected. In the high *Ra* limit, Θ_{av} tends to the arithmetic average of the temperatures of the sources, irrespective of their areas. In analogy with a stirred tank, the rapid growth of Θ_{av} with *Ra* reflects the high degree of fluid mixing, and the highly convective flow that exist at high *Ra*. However, starting from the lower Rayleigh number limit (10^3), Θ_{av} shows an initial *decrease* with increasing *Ra*, passes through a minimum at $Ra = 10^5$ for all values of s/L, then increases with further increments in *Ra*. The initial decrease of Θ_{av} is counter-intuitive, and depends on the difference in the active areas, as it does not occur at all in the test case. Also, the effect is not specifically related to the three-dimensionality of the flow. This is suggested by the fact that two-dimensional runs conducted for a square cavity with a hot strip of $s/L = 0.5$ centered on a vertical wall, and a fully cooled opposite wall, resulted in average temperatures which also had a minimum at $Ra = 10^5$ (Table 1). The variation of Θ_{av} with *Ra* in these test runs was less pronounced than in the three-dimensional case. If Θ_{av} is used as an index of the temperature field, the analogy that it reveals between the three-dimensional and two-dimensional cases on the one hand, and the symmetry of the flow and temperature fields with respect to the plane $Z = 0.5$ on the other, make it possible to characterize the evolution of the temperature field with *Ra* by studying these fields in the symmetry plane.

Undoubtedly, the behavior of Θ_{av} can be related to the energy transfer as seen by the close correspondence between Figs. 2 and 3. Also, its variations reflect the degree of thermal stratification in the enclosure, as shown in the following. Fig. 4 shows the velocity vectors at $Z = 0.5$ for three Rayleigh numbers, for $s/L = 0.3$, in the three-dimensional case. The flow in this plane consists of a main circulation cell with secondary loops. The main cell is similar to the one observed in the test problem (de Vahl Davis circulation), especially at $Ra = 10^3$ (Fig. 4(a)). However, at a high Rayleigh number, the difference in the active areas causes a shorter ascending path of the fluid adjacent to the hot

Table 1
Two-dimensional average temperature and Nusselt number results for a square cavity with a heated strip of $s/L = 0.5$ as a function of the Rayleigh number

Ra	Θ_{av}	*Nu*
10^3	−0.0509	1.0003
10^4	−0.0806	1.8309
10^5	−0.0987	3.4549
4×10^5	−0.0902	5.1668
10^6	−0.0753	6.7876

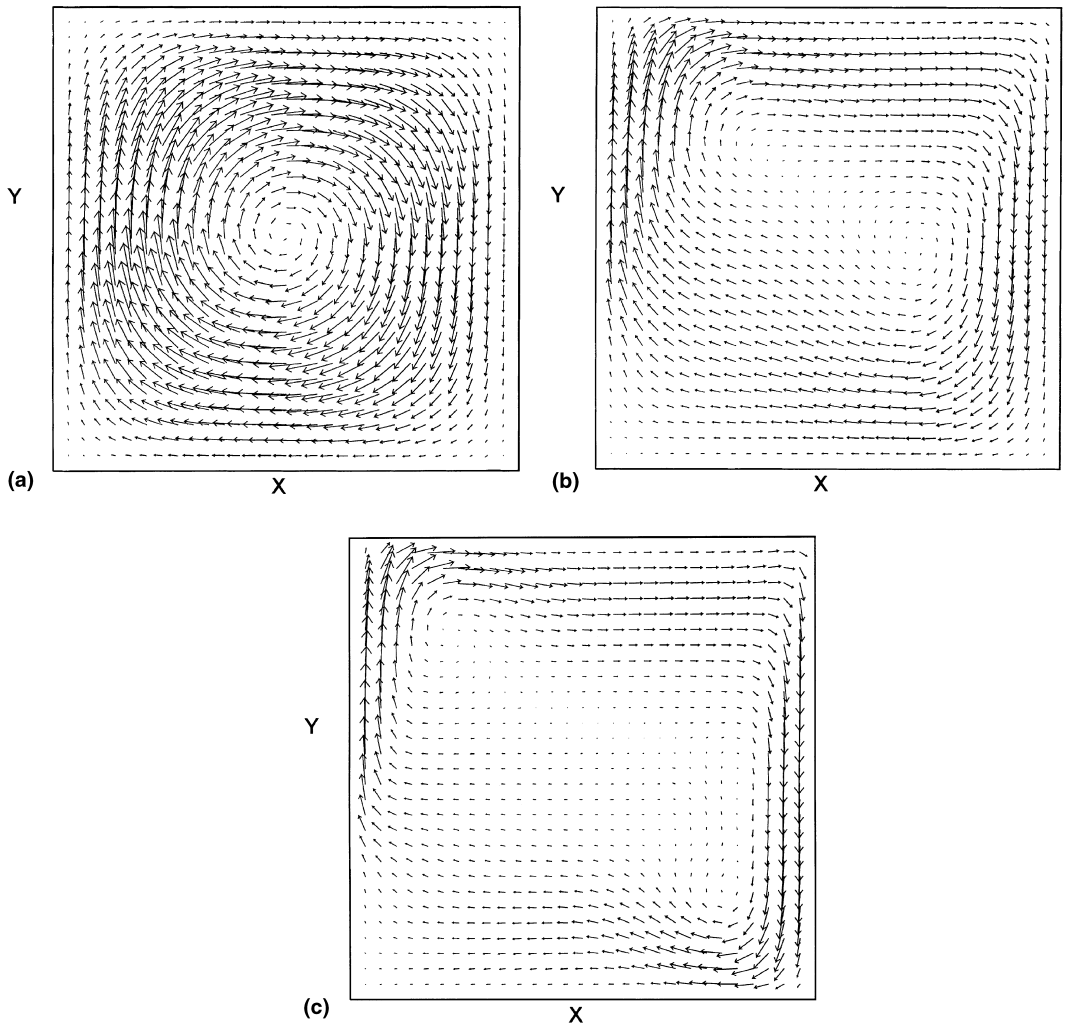

Fig. 4. Velocity vectors in the plane $Z = 0.5$, $s/L = 0.3$: (a) $Ra = 10^3$; (b) $Ra = 10^5$; (c) $Ra = 10^6$.

sector. In the central zone, the fluid is almost stagnant, as in the test problem. The cold fluid expands vertically after leaving the cold wall, and is directed toward the zone of positive buoyancy. As in the test problem, centers of rotation develop at the upper left and lower right of the enclosure (Figs. 4(b) and (c)).

Fig. 5 shows isotherms at $Z = 0.5$ for three Rayleigh numbers and $s/L = 0.3$. At $Ra = 10^3$, (Fig. 5(a)) isotherms closely resemble the pattern observed in the test problem at low Ra. They are nearly vertical in most of the enclosure, they deflect in the direction of movement, and the differences with respect to the test case are confined to the vicinity of the hot source, from where heat flows radially by conduction. At $Ra = 10^5$ (Fig. 5(b)), the increase in vertical velocities has defined zones of advancing motion at the top and bottom of the enclosure, as seen in Fig. 4(b), where heat transfer is essentially by convection, with thermal stratification and boundary layers on the active zones, especially on the hot one. In this stratified pattern, the isotherms for $\Theta > 0$ are confined to a very small region near the wall containing the hot source. The cross-sectional area occupied by the fluid at temperatures in excess of $\Theta = 0$ is clearly smaller in Fig. 5(b) than in Fig. 5(a). Therefore, the average fluid temperature for the whole enclosure is lower than in Fig. 5(a).

U and V velocities for this case are still low (Table 2), because of the reduced area of the hot source. Most of the conduction paths in a large central zone have been nearly suppressed as the horizontal temperature gradients are extremely low because of stratification. This fact, added to the evidence of a still weak convection, not strong enough to promote a high convective contribution to heat transfer, accounts for the reduction in average temperature when the Rayleigh number increases from 10^3 to 10^5. The weakness of the convection

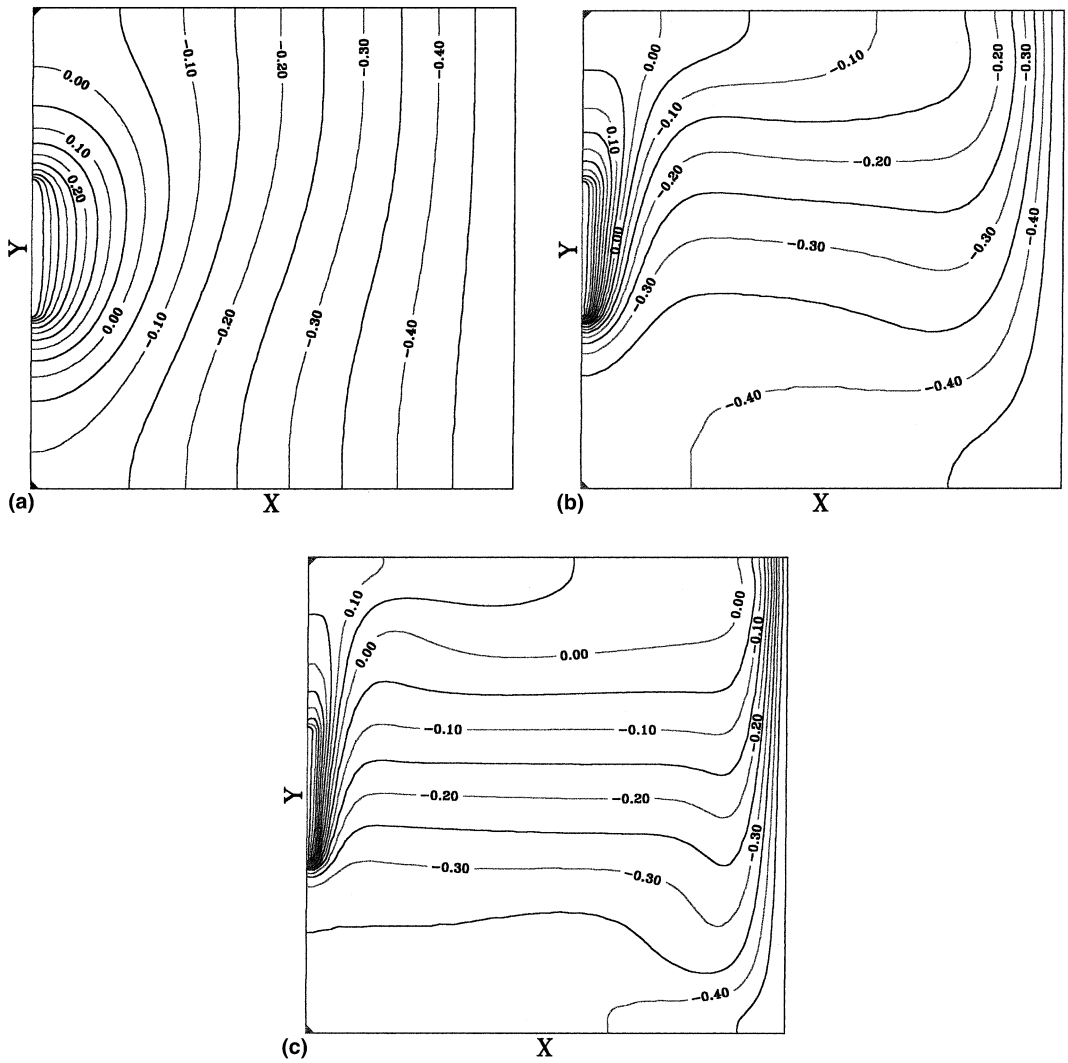

Fig. 5. Isotherms in the plane $Z = 0.5$, $s/L = 0.3$: (a) $Ra = 10^3$; (b) $Ra = 10^5$; (c) $Ra = 10^6$.

Table 2
Values of the maximum U and V velocities in the mid-plane $Z = 0.5$ for different values of s/L as a function of the Rayleigh number

Ra	$s/L = 0.3$		$s/L = 0.5$		Test	
	U	V	U	V	U	V
10^3	2.0317	2.7616	2.8744	3.3107	3.5013	3.5172
10^4	11.8233	16.3610	14.7987	18.8105	16.9618	18.9757
10^5	27.7406	54.2463	35.9146	63.2177	39.1161	65.8418
10^6	58.3830	151.6931	79.6175	182.0397	70.8639	218.0688

generated at Rayleigh numbers up to 10^5 can be demonstrated by noting that the maximum vertical and horizontal velocities in the $Z = 0.5$ plane at $s/L < 1$ are lower than in the test problem. (Table 2). The reduction in the U velocity component relative to the test case, accounts for the lower overall heat transfer observed. The U value is, however, higher than that for the test problem from a Rayleigh number of 10^6.

A change of regime occurs at $Ra > 10^5$. As Fig. 5(c) shows, at $Ra = 10^6$, the zone of temperatures above 0.0 has greatly increased in area, and the isotherm $\Theta = 0$ is included as one of the stratified temperature levels. The

maximum U has increased with respect to its counterpart for the test problem (Table 2). Conduction is still less significant than in Fig. 5(b). The convective process has gained importance, and reflects itself in increases in average temperature and heat transfer. Similar characteristics are found for the isotherms near the lateral walls (not shown).

To sum up, at $Ra = 10^3$, heat flows between the sources by conduction using all possible paths available in the enclosure volume. At a slightly higher Ra, incipient convection sets in, in which directions of convective heat flow appear at the enclosure top and bottom. This causes thermal stratification and suppression of conduction paths. The resulting heat transfer between the sources now depends almost entirely on the localized zones of advance of the fluid from the hot towards the cold source and vice-versa. These advance velocities are still weak, so they do not compensate for the loss of the conduction contribution to heat transfer. This fact is reflected in the decrease in average fluid temperature. In the test problem, the decrease in conduction during the transition is exactly compensated by increases in convection, and this gives the Nu–Ra curve the appearance of a fully convective regime from $Ra = 10^3$ on.

From the above, it is necessary to admit that a fully convection-dominated regime exists only from a Rayleigh number of 10^5 on. Nusselt–Rayleigh relationships in this convective regime are given in Table 3. Fusegi's results and our results in the ranges of Ra for which convection prevails can be represented by power laws of the type $Nu = C\ Ra^n$. The exponents for $s/L = 1$ and 0.7 are essentially equal. It is therefore expected that for $s/L > 0.7$, there will be only small variations in C. This is not the case with the lower values of s/L, for which a definite increase in the Rayleigh number exponent with s/L is observed. An explanation of this effect is needed.

The conclusions so far arise from an analysis of temperatures and velocities in the plane $Z = 0.5$, and hold for features which are common to our problem and to its nearest two-dimensional counterpart. Now, it is necessary to consider the three-dimensional aspects of the flow. Isotherms in planes parallel to the hot surface are shown in Figs. 6(a)–(c), for $s/L = 0.3$. They show that buoyancy is generated by the hot surface, but not by its passive sides. In the isograms at $X = 0.025$, the source is delineated by the isotherms. At low Ra (Fig. 6(a)), the isotherms show radial conduction from the hot source, while at a higher Ra (Fig. 6(b)) conduction has been suppressed. Strong temperature gradients appear at the heater bottom, where cold fluid reaches the hot zone. Isotherms at the sides of the hot source are stratified, suggesting that the ascending movement, which is very intense, is significant only in front of the heater. The anticipated temperature symmetry with respect to $Z = 0.5$ is demonstrated by Figs. 6(a) and (b). Isotherms near the cold wall show a regular pattern of stratification (Fig. 6(c)).

Table 3
Coefficients and exponents of the relationship $Nu = C\ Ra^n$ in the convective regime as a function of s/L

Case	C	n	Ra range
Fusegi et al. [1]	0.1309	0.3040	10^3–10^7
$s/L = 0.7$	0.1121	0.2988	10^5–10^7
$s/L = 0.5$	0.0564	0.3276	10^5–10^7
$s/L = 0.3$	0.0115	0.4136	10^5–10^7

Fig. 7 shows velocity vectors at $s/L = 0.3$. The flow pattern is symmetric with respect to $Z = 0.5$. The main cell is similar to the one observed in the test problem, as already seen in Fig 4. At low Ra (Fig. 7(a)), the velocities, which are very low, are fairly uniform near the hot wall, except at the sides $Z = 0$ and $Z = 1$ because of wall friction. This pattern changes notoriously at higher Ra (Figs. 7(b) and (c)), where the high buoyancy exerted by the heater at $X = 0$, causes high velocities of ascension only in front of it, while near the passive sides, the velocities are much lower. Descending velocities are rather uniform near $X = 1$, where there is negative buoyancy all across the wall (Fig. 7(d)).

In Figs. 4(b) and (c), an upward movement of the cold stream returning to the hot wall from the cold one was seen. The locally low level of buoyancy below the hot sector allows this vertical expansion. The general circulation pattern is deformed relative to the test case, because at high Ra, the ascending flow near the hot wall accommodates to the size and shape of the hot sector, and the zone of descending flow has essentially the dimensions of the cold zone (Figs. 7(a)–(d)). Therefore, vertical and lateral expansions and contractions of the stream connecting the active zones take place. This distortion of the main circulation is more notorious at low values of s/L and at high Ra. Fig. 8 shows a succession of velocity patterns at $Ra = 10^6$, at increasing values of X. In the upper part of the diagrams, for low values of X, the fluid heated by the hot wall expands laterally outwards as it advances along X. This expansion is still very marked at $X = 0.5$. After the expansion is completed ($X > 0.5$), the hot fluid flows nearly parallel to the X axis, to reach the cold wall, at which the flow descends all along the Z axis (Fig. 7(d)). The return of the cooled fluid from the enclosure bottom takes place as a combination of ascending movement (Fig. 4) and lateral inward displacement toward the $Z = 0.5$ plane (Figs. 8(b) and (c)). The fluid below $Y = 0.5$ converges to the hot sector, to be ultimately raised by the buoyancy force at the hot source, to start the cycle again. This behavior is reflected in the extreme values of velocities. For all values of s/L, at $Ra = 10^3$ and 10^4, the absolute maximum velocities U and V occur at the plane of symmetry $Z = 0.5$, at the lines defined by this plane and the planes $X = 0.5$ and $Y = 0.5$, respectively, as in the test problem. For higher Ra, the maxima, while still located

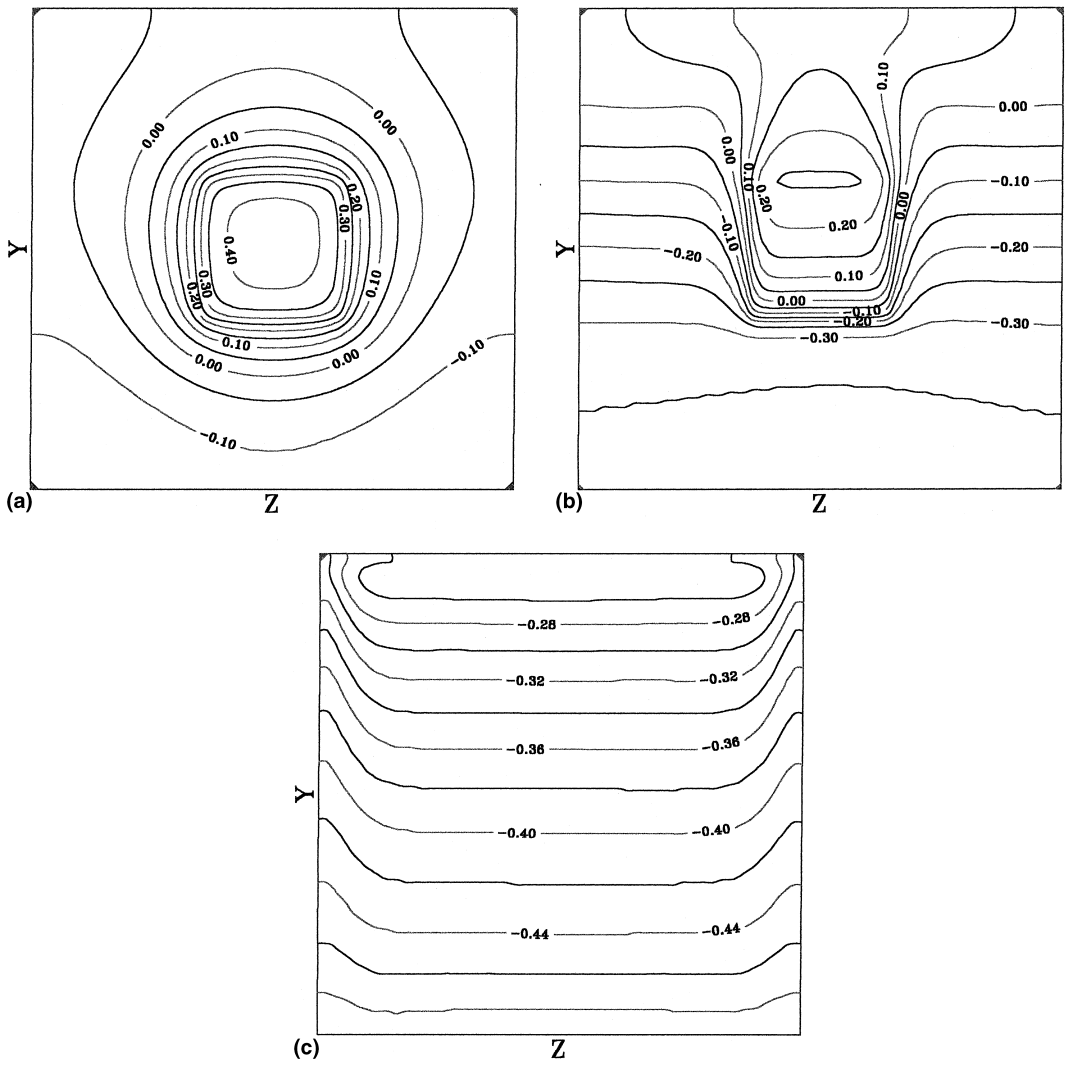

Fig. 6. Isotherms in the vicinity of the active walls, for $s/L = 0.3$: (a) $X = 0.025$; $Ra = 10^3$; (b) $X = 0.025$, $Ra = 10^6$; (c) $X = 0.975$, $Ra = 10^6$.

in the plane $Z = 0.5$, are displaced to other positions within that plane ($X < 0.5$), and show great increases with respect to the velocity values at the more symmetric positions detailed above. These effects are caused by the expansion/contraction behavior of the main circulation cell.

The three-dimensionality of the flow, shown in the above figures for $Ra = 10^6$, develops during the transition ($10^3 \leqslant Ra \leqslant 10^5$). As Ra is increased, the lateral velocity component (W), which is small at low Ra, increases markedly, becoming comparable with the maximum velocity components U and V (Table 4). Beyond $Ra = 10^5$, however, the percent increase in W with respect to U and V is low. This indicates that a final degree of fluid mixing in the enclosure has been nearly attained about $Ra = 10^5$. This is an additional argument to support the claim that a fully convective regime starts at that particular value of Rayleigh number. The increase in W with Ra is caused by the fact that, as buoyancy force increases, the flow raised by the hot source and restricted by the horizontal wall, finds an additional way to leave the hot zone, which is a lateral movement toward the planes $Z = 0$ and $Z = 1$. As Ra grows, the lateral diversion of this flow gains importance, (Figs. 7(a)–(c)) aided by the reduced buoyancy at both sides of the hot source. This lateral movement, superposed to advance along the X-direction, will ultimately be responsible for the mixing of the fluid in the whole enclosure, and manifests itself as increases in Θ_{av} and Nusselt number.

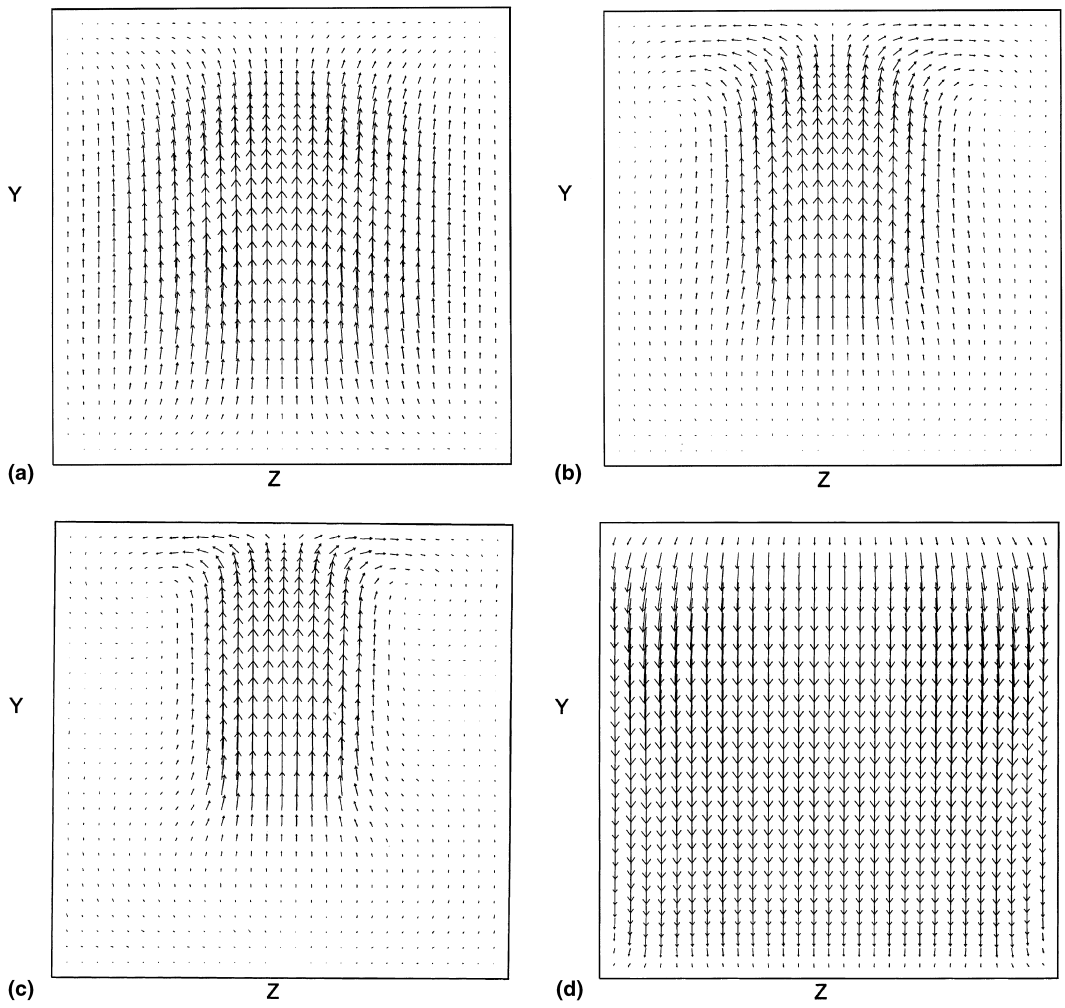

Fig. 7. Velocity vectors in the vicinity of the active walls, for $s/L = 0.3$: (a) $X = 0.025$, $Ra = 10^3$; (b) $X = 0.025$, $Ra = 10^5$; (c) $X = 0.025$, $Ra = 10^6$; (d) $X = 0.975$, $Ra = 10^6$.

The absolute maxima in velocities in the test problem for $Ra = 10^6$ are $U = 127.602$ and $V = 214.608$ (our results). At the same Ra in our problem, as a result of expansions and contractions, the maximum U is higher than, or comparable to, that of the test problem for $s/L = 0.5$ and 0.3 (140.657 and 119.045, respectively). Conversely, the maximum V in the present problem (201.595 and 195.635) is always lower than that in the test problem. As vertical velocity is mainly determined by the heater height, values higher than those for the test case cannot appear in our problem at any given Ra. However, the horizontal velocities are determined by the inertia forces, therefore, as the stream is contracted to reach the heater, the accommodation of the flow for returning to the cold surface, will generate higher X-component velocities near the top of the hot zone.

In the test problem, [1,2] a regime change, consisting of an increase in flow three-dimensionality, also occurs around $Ra = 10^5$. At $Ra < 10^5$, the flow is nearly two-dimensional, with maximum U and V in $Z = 0.5$. At higher Ra, three-dimensional effects become important, and the maxima in U and V occur near the lateral walls. This results from the fact that, at high Rayleigh numbers, with high velocities, the flow can no longer keep uniform conditions along Z: zero velocities appear at $Z = 0$ and $Z = 1$, because of wall friction. Some fluid is therefore displaced inwards, where it is dragged by the main motion and contributes to the maximum velocities found outside the plane of symmetry. This effect does not propagate to the mid-plane $Z = 0.5$, where velocities keep the levels of the two-dimensional problem, although slightly reduced. As already said, in the test problem, the Nu–Ra curves suggest a convective

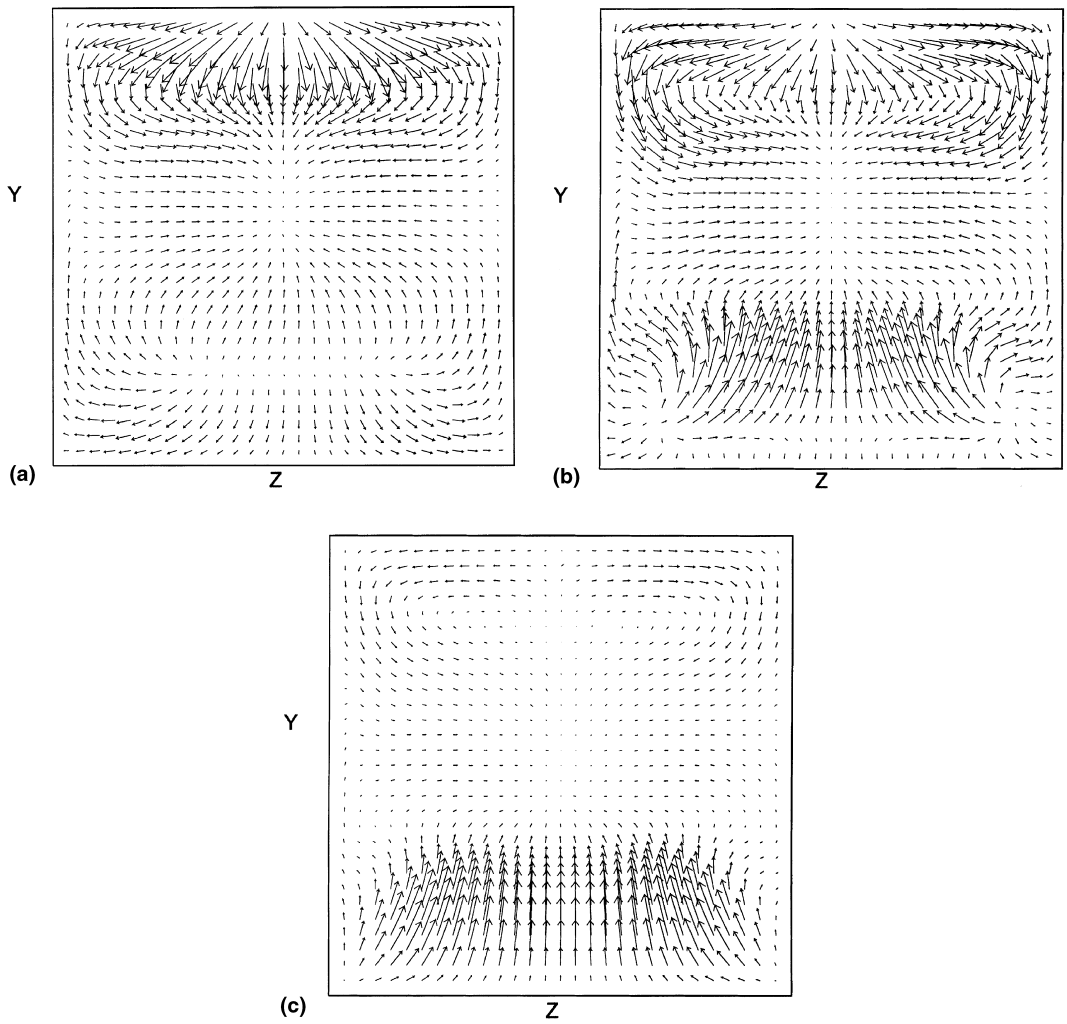

Fig. 8. Velocity vectors at various positions along the X-axis, for $s/L = 0.3$ and $Ra = 10^6$: (a) $X = 0.34$; (b) $X = 0.5$; (c) $X = 0.64$.

Table 4
Maximum lateral velocities (W) at different Rayleigh numbers as a percentage of the maximum U and V velocities for $s/L = 0.3$ as a function of the Rayleigh number

Ra	W_{max} as a percent of:	
	U_{max}	V_{max}
10^3	11.82	8.99
10^4	27.87	19.08
10^5	56.26	32.06
4×10^5	59.85	35.45
10^6	61.17	37.56

behavior from $Ra = 10^3$. This is because equally sized active sources allow a gradual change from conductive to convective dominance. The present case, characterized by early suppression of conduction and slow development of convection (in the range of Ra) because of the reduced buoyancy, only allows to consider the regime as truly convective from a Rayleigh number of 10^5 on.

5. Conclusions

The natural-convection in cubical enclosures with vertical, square, frontally opposed sources of different sizes and temperatures was studied. For all values of the heater side to cavity side ratio, a symmetric, single circulation cell connects both sources. The transition to convective regime occurs in the range of Ra from 10^3 to 10^5. At low Rayleigh numbers, an imbalance between the superposed effects of conduction and incipient convection is reflected in a slow approach to the convective

regime. The transition ends at $Ra = 10^5$. In the test problem, a change of regime has also been found at this particular value of Rayleigh number. At $Ra > 10^5$, a high degree of fluid mixing is observed in the enclosure, caused by fully three-dimensional convection. At high Ra, the circulation undergoes changes in cross-section, adapting itself to the size of the sources with changes in flow direction, which at $Ra > 10^5$, result in a highly three-dimensional flow, with high lateral velocity components. This flow pattern does not allow heat transfer levels as high as in the test case, but promotes fluid mixing in the whole enclosure.

References

[1] T. Fusegi, J.M. Hyun, K. Kuwahara, B. Farouk, A numerical study of three-dimensional natural-convection in a differentially heated cubical enclosure, Int. J. Heat Mass Transfer 34 (6) (1991) 1543–1557.

[2] R.J.A. Janssen, R.A.W. Henkes, C.J. Hoogendoorn, Transition to time-periodicity of a natural-convection flow in a 3D differentially heated cavity, Int. J. Heat Mass Transfer 36 (11) (1993) 2927–2940.

[3] T. Lee, T.F. Lin, Three-dimensional natural convection of air in an inclined cubic cavity, Numer. Heat Transfer, Part A 27 (6) (1995) 681–703.

[4] R.L. Frederick, Some cases of transition from conduction to convection regimes in natural convection in cubical enclosures, in: T. Ito, E. Bilgen (Eds.), Proceedings of the Third International Thermal Energy Congress, Kitakyushu, Japan, 1997, pp. 116–122.

[5] R.L. Frederick, Natural convection heat transfer in a cubical enclosure with two active sectors on one vertical wall, Int. Commun. Heat Mass Transfer 24 (4) (1997) 507–520.

[6] T.J. Heindel, S. Ramadhyani, F.P. Incropera, Conjugate natural convection from an array of protruding heat sources, Numer. Heat Transfer Part A 29 (1) (1996) 1–18.

[7] D.E. Wroblewski, Y. Joshi, Liquid immersion cooling of a substrate-mounted protrusion in a three-dimensional enclosure: the effects of geometry and boundary conditions, J. Heat Transfer 116 (1) (1994) 112–119.

[8] L. Tang, Y. Joshi, Application of block-implicit multigrid approach to three-dimensional heat transfer problems involving discrete heating, Numer. Heat Transfer Part A 35 (7) (1999) 717–734.

[9] D. Poulikakos, Natural convection in a confined fluid-filled space driven by a single vertical wall with warm and cold regions, J. Heat Transfer 107 (4) (1985) 867–876.

[10] D. Kuhn, P.H. Oosthuizen, Unsteady natural convection in a partially heated rectangular cavity, J. Heat Transfer 109 (3) (1987) 798–801.

[11] B.L. Turner, R.D. Flack, The experimental measurement of natural convective heat transfer in rectangular enclosures with concentrated energy sources, J. Heat Transfer 102 (2) (1980) 236–241.

[12] F.K. Gatheri, J.A. Reizes, E. Leonardi, G. de Vahl Davis. Natural convection in an enclosure with localized heating and cooling: a numerical study, in: G.F. Hewitt (Ed.), Proceedings of the 10th International Heat Transfer Conference, Brighton, UK, 1994, pp. 361–366.

[13] S.V. Patankar, Numerical Heat Transfer and Fluid Flow, Hemisphere, Washington, DC, 1980 (Chapter 4).